FEBS Letters 580 (2006) 2488–2494

Water molecules as structural determinants among prions of low sequence identity

Alfonso De Simone[a,b], Guy G. Dodson[a,c], Franca Fraternali[a,d,*], Adriana Zagari[b,e,*]

[a] National Institute for Medical Research, The Ridgeway, Mill Hill, NW7 1AA, London, UK
[b] Dipartimento delle Scienze Biologiche, Sezione Biostrutture and CNISM, Università di Napoli Federico II, Via Mezzocannone 16, I-80134 Napoli, Italy
[c] York Structural Biology Laboratory, University of York, York YO10 5YW, UK
[d] The Randall Centre for Molecular Mechanisms of Cell Function, King's College London, New Hunt's House, Guy's Campus, London SE1 1UL, UK
[e] Istituto di Biostrutture e Bioimmagini, CNR, via Mezzocannone 16, I-80134 Napoli, Italy

Received 27 December 2005; revised 9 February 2006; accepted 9 February 2006

Available online 17 April 2006

Edited by Hans Eklund

Abstract **The nature of the factors leading to the conversion of the cellular prion protein (PrP^C) into its amyloidogenic isoform (PrP^{Sc}) is still matter of debate in the field of structural biology. The NMR structures of non-mammalian PrP^C (non-mPrP) from frog, chicken and turtle [Calzolai, L., Lysek, D.A., Perez, D.R., Guntert, P. and Wuthrich, K. (2005) Prion protein NMR structures of chickens, turtles, and frogs. Proc. Natl. Acad. Sci. USA 102, 651–655] have provided some new and valuable information on the scaffolding elements that preserve the PrP^C folding, despite their low sequence identity with the mammalian prions (mPrP). The present molecular dynamics study of non-mPrP^C focuses on the hydration properties of these proteins in comparison with the mammalian ones. The data reveal new insights in the PrP hydration and focus on the implications for PrP^C folding stability and its propensity for interactions. In addition, for the first time, a role in disfavoring the PrP^C aggregation is suggested for a conserved β-bulge which is stabilized by the local hydration.**

Keywords: Prion protein; Protein hydration; Molecular dynamics; Edge-to-edge aggregation; Structural comparison

1. Introduction

The cellular prion protein (PrP^C) is a monomeric glycoprotein (~210aa in the mature form) composed of a flexible N-terminal region and a globular C-terminal domain of three α-helices (H1, H2 and H3) and a short double stranded antiparallel β-sheet (β1 and β2). As yet the PrP^C function(s) is(are) not known [1]. Extracellular deposition of insoluble PrP amyloid fibrils apparently occurs at the onset of transmissible spongiform encephalopathy (TSE), a group of fatal neurological disorders also known as "prion diseases" [2,3].

It is now established that the normal (cellular) form of prion (PrP^C) converts into an amyloidogenic isoform (PrP^{Sc}) with structural differences [4] that favor its ready aggregation to amyloid fibrils [5–7]. However the structural pathway from PrP^C to PrP^{Sc}, and the molecular basis of the subsequent fibrils formation, are poorly understood [8–10]. One factor that is important in the process is the nature of the prion's hydration and its role in the stability of PrP. As elegantly showed by Fernandez et al., amyloidogenic proteins and especially PrP^C have a large number of defectively wrapped hydrogen bonds [11–14]. These backbone hydrogen bonds are poorly protected against water interaction by flanking hydrophobic residues.

High-pressure calorimetry studies have revealed that alterations in the PrP hydration occur by passing from PrP^C to PrP^{Sc} [15]. Interestingly, solvent environment has been showed to tune the amyloidogenesis of insulin [16].

In a previous study, based on molecular dynamics (MD) simulations, we pointed out the special hydration properties at the surface of the human (huPrP) and sheep (shPrP) prions [17]. The calculations characterized protein surfaces where tightly bound waters (referred as to "sharp spots") evidently add to the local structural stability. Equally the hydration maps identified specific surfaces where main chain H-bonds are surrounded by very mobile bulk-like water (referred as to "smooth spots"). These regions might exhibit energetically close alternative patterns of H-bonding effectively modulating the local structural stability and thereby favoring unfolding and aggregation events [17].

Recently, Calzolai et al. [18] have resolved the NMR structures of PrPs from chicken (chPrP), turtle (tPrP), and frog (xlPrP). These three proteins share about 30% of sequence identity with the better known mammalian PrPs (mPrPs), which themselves form a conserved group of PrPs with about 90% of sequence identity. The newly resolved non-mammalian prion structures show the general features of the PrP^C-fold; that includes a mobile disordered N-term tail and a globular C-term domain. In particular the structural comparison shows that in non-mPrPs the secondary structure elements are moderately conserved, while the major structural variability is found in the H1 packing and in some connecting loops (see Supplementary Fig. 1). As result of a detailed analysis of the sequences and the structural comparisons, scaffolding residues, important for preserving the PrP^C-fold, were identified.

*Corresponding authors.
E-mail addresses: ffranca@nimr.mrc.ac.uk (F. Fraternali), zagari@chemistry.unina.it (A. Zagari).

Abbreviations: MD, molecular dynamics; MDHS, molecular dynamics hydration sites; PrP, prion protein; PrP^C, cellular PrP; PrP^{Sc}, scrapie PrP; huPrP, human PrP; shPrP, sheep PrP; chPrP, chicken PrP; tPrP, turtle PrP; xlPrP, frog PrP; mPrP, mammalian PrP; RMSD, root mean square deviation

0014-5793/$32.00
doi:10.1016/j.febslet.2006.02.083

In the present study we have extended our analysis of mPrP hydration to the three non-mammalian prions: chPrP, xlPrP and tPrP. Taking advantage from data calculated for various low sequence identity PrPs, our analysis points out significantly conserved hydration patterns. The results are discussed in terms of folding stability and propensity for protein–protein interaction.

2. Methods

2.1. Molecular dynamics set-up

Several MD simulations in explicit solvent have been performed on the C-term globular domains of different non-PrPs NMR structures: chPrP(126–242), xlPrP(125–226) and tPrP(119–225) (pdbcode: 1U3M, 1XU0 and 1U5L, respectively) [18]. As a reference for mPrPs, the shPrP(125–230) X-ray crystal structure (pdbcode: 1UW3) [19] was selected. Throughout this paper the huPrP residue numbering is adopted for mPrP (consistently with the 1UW3 crystal structure). The MD trajectories were used for calculating the water distribution around the proteins. All the simulations were performed with the GROMACS [20] package by using GROMOS96 [21] force field. A time step of 2 fs was used. The trajectories have been saved every 250 steps (0.5 ps). The systems were simulated in an NPT ensemble by keeping constant the temperature (300 K) and pressure (1 atm); a weak coupling [22] to external heat and pressure baths were applied with relaxation times of 0.1 ps and 1 ps, respectively. The initial shortest distance between the protein and the box boundaries was 1.5 nm. The remaining box volume was filled with extended single point charge (SPCE) water model [23]. Bonds were constrained by LINCS [24] algorithm. Non-bonded interactions were accounted by using the particle mesh Ewald method (PME, grid spacing 0.12 nm) [25] for the electrostatic contribution and cut-off (14 Å) for Van der Waals contribution. The protonation states of pH sensitive sidechains were as follows: Arg and Lys were positively charged, Asp and Glu were negatively charged and His was neutral. A system of neutral charge was achieved by adding Na^+ ions. The simulations have been carried out for a time of 10 ns. Root mean square deviations (RMSDs) vs. time have been calculated on C^{α}-atoms for all PrP structures with and without loops (see Supplementary Fig. 2). As can be seen from the plots, all the systems converge to a plateau after about 2 ns. The subsequent stationary sampling (~8 ns) has been considered sufficiently long for the purpose of a hydration analysis. Further simulation details are summarized in Table 1.

2.2. Water density function

Our hydration analysis is largely based on the solvent density map [17,26,27] whose maxima are assumed to be the molecular dynamics hydration sites (MDHS). The space surrounding the protein is divided in two shells: the first describes the water around the protein and comprises the region within a distance of 0.6 nm from the protein surface. The second shell extends from 0.6 nm to 0.8 nm from the protein surface and represents the bulk solvent shell. The solvent density calculation is grid based (step-size 0.05 nm). To avoid the noisiness produced by protein translation and rotation, for each frame the atom coordinates are transformed by superimposing the current model onto a reference one. The local maxima of the density function (MDHS) are searched following the restrictions to be the highest value in a radius of 0.14 nm with a minimum density of 1.7 times the value of bulk water. Subsequently, MDHS are classified on the basis of the water residence time calculated through the time autocorrelation function.

2.3. Time autocorrelation function and residence time

The time autocorrelation function $P(\tau)$ [26] provides the probability of finding the same water in the hydration site at two different times t, $t + \tau$. The adopted formula is:

$$P(\tau) = \sum_t \delta(W(t), W(t+\tau))$$

where the delta function $\delta(W(t), W(t+\tau))$ assigns 1 or 0 whether the same water is (or is not) found in the hydration site at times t and $t + \tau$. The $P(\tau)$ curve is then fitted by a single exponential decay providing the residence time.

2.4. Calculation of the free energy of water binding

The free energy difference between two states a and b of the system is calculated with the double-decoupling method [28]. This method divides the binding process into two steps; as first, a water molecule is transferred from the bulk solvent to the gas phase (no intermolecular interactions); subsequently, it is relocated into the binding site where it is allowed to optimize the native interactions. Both the contributions are calculated with the slow growth method.

The derivate of the free energy with respect to the reaction coordinate "λ" (which is 0 in the state a and 1 in the state b) is computed according to the formula:

$$\frac{dG}{d\lambda} = \left\langle \frac{\partial H(\boldsymbol{p}, \boldsymbol{q}, \lambda)}{\partial \lambda} \right\rangle_{\lambda}$$

where $H(\boldsymbol{p},\boldsymbol{q},\lambda)$ is the classical Hamiltonian and $\boldsymbol{p}$ and $\boldsymbol{q}$ are the Cartesian coordinates and the conjugate momenta, respectively.

2.5. Linear hydration function

The linear hydration function (LHF) assigns a certain hydration value to each residue of the protein. As first each MDHS is assigned to the nearest residue. Then, the LHF is calculated according to the formula:

$$\mathrm{LHF}_{aa} = N \sum_{j=aa-2}^{j\leqslant aa+2} \left(\sum_i \frac{\rho_i}{d_i} \Big/ \mathrm{SASA}_{aa} \right)$$

where N is a normalization coefficient introduced to ensure an adimensionality and a curve area of 1. The "j" sum indicates that plot is drawn by means of a sliding window of five residues. The "i" sum is computed over the hydration sites corresponding to the residue; "d" is the distance from the nearest protein atom and "ρ" is the relative density of the hydration site. SASA is the surface accessibility of the residue (POPS server [29]).

Table 1
Parameters of the simulations

	shPrP	chPrP	tPrP	xlPrP
Structure pdbcode	1UW3	1U3M	1U5L	1XU0
Charge neutralizing ions	2 Na^+	1 Na^+	2 Na^+	–
Starting box size (Å)	$64.3 \times 63.9 \times 81.3$	$74.5 \times 74.9 \times 65.3$	$77.9 \times 64.1 \times 58.9$	$78.3 \times 67.8 \times 59.0$
Water molecules	10489	11598	9286	9895
Energies (kJ/mol)				
Protein–protein (total)	−10292.79	−10561.47	−9690.13	−9446.58
Protein–protein (LJ)	−3901.27	−4047.42	−3713.12	−3653.62
Protein–protein (El)	−6391.52	−6514.05	−5977.01	−5792.96
Protein–solvent (total)	−10372.21	−11603.65	−10151.91	−10643.94

3. Results and discussion

3.1. Structurally conserved waters in PrPs

The analysis of huPrP and shPrP hydration [17] showed a good correlation between MDHS with high residence time (>1 ns) and the crystallographically observed water molecules that are conserved among the known X-ray structures. One of these waters (W1) is of particular interest because it bridges three protein regions belonging to different secondary structural elements (β1, β2 and H3). This water mediates the interaction between the amide of V161 (β2, huPrP numbering) and the carbonyl of S132, thus stabilizing the β-bulge (βb1) that follows the β1 (Fig. 1A) [17]; additionally it makes a H-bond with the Q217(H3) sidechain (TSE sensitive [30]). Other residues also participate in the binding-site framework: the sidechain of Q160 prevents the natural elongation of the β-sheet by interacting with the carbonyl of G131 (β1, TSE sensitive [31]), and preventing the extension of the β-sheet to the V161 peptide. Moreover R220 sidechain interacts with S132 OG sustaining the bulge promoted by the G131 (Fig. 1A).

Considerable sequence variations are observed in the non-mPrPs in contrast to the closely conserved mPrPs. These variations, especially the ones on the protein surface, are likely to influence the distribution and the character of the hydration sites. In particular, the above described water binding site (Fig. 1A) was expected to adopt a different framework in non-mPrP since it is located next to the variable loops that determine the H1 packing diversity. Notably, we found that this water binding site is significantly conserved in all the non-mPrPs (Fig. 1). Indeed, during the dynamic calculations, the water molecule (W1) is seen to be trapped in the site where it remains for the entire simulation. This conservation is singular since this is the only hydration site that is conserved among mPrPs and non-mPrPs.

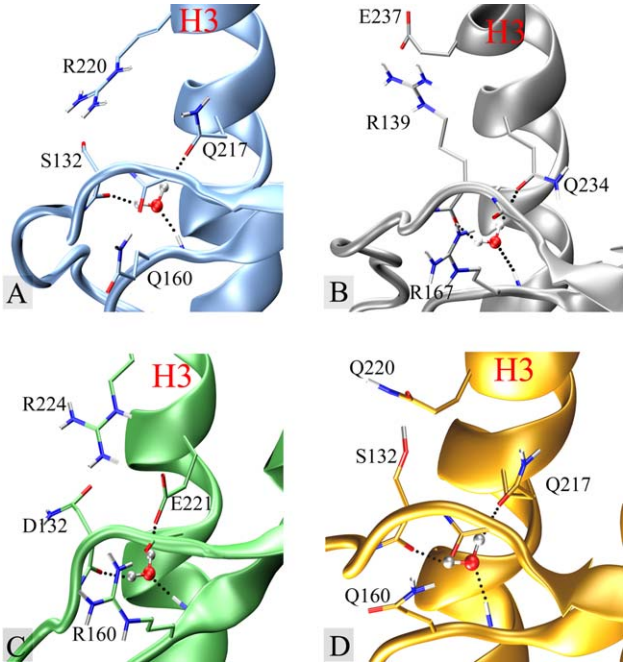

Fig. 1. Close up view of the water-binding site in the performed MDs. Interestingly, the water is conserved among non-mPrP. Remarkably, despite the sequence differences, the water-mediated interaction between sidechains of the residues following G131 (huPrP numbering) and a residue from the H3, is preserved. This interaction evidently contributes to the bulge stability. (A) shPrP, (B) chPrP, (C) xlPrP, (D) tPrP.

These data reinforce the idea that a bound water molecule in this region is an important element in the PrP^C-fold. According to the significant conservation among the PrPs, the hydration site should be considered an additional scaffolding determinant for preserving the PrP^C-fold [18]. We also suggest (vide infra) a specific structural/functional role of the hydration site and the connected β-bulge βb1.

3.2. Role of βb1

The model of intermolecular β-sheet formation is believed to be a widespread mechanism of protein aggregation [32]. Analyzing non-aggregating proteins, Richardson & Richardson (R&R) [33] have identified natural structural features that inhibit the β-sheets edge-to-edge aggregation. In particular, they propose that structural irregularities, such as a β-bulge promoted by a glycine in the last position of the strand (see Supplementary Fig. 3), have been "negatively designed" to lower the edge strands propensity to engage intermolecular β-sheets. Following the R&R rules [33], we suggest that βb1 has the properties of such anti-aggregating elements.

There are several data supporting this idea. The glycine that precedes and promotes the bulge (i.e., G131 in shPrP) is perfectly conserved among PrPs whereas the following residue is variable; a similar structural pattern is also discussed by R&R, i.e., in the β-propeller [33] (see Supplementary Fig. 3A). It should be noted that, in PrPs, this sequence variability does not disrupt an interaction with a residue from H3 that is essential for the bulge stability [17], i.e., S132-R220 in shPrP or R139-E237 in chPrP (Table 2 and Fig. 1). In addition, localized human pathological mutations like the G131V [31,34] (Creutzfeldt–Jakob disease) and Q217R [30,35] (Gerstmann–Sträussler syndrome) are known; these mutations are likely to exert a disruptive influence on the bulge (as shown by the Q217R MD simulation [17]).

Is the βb1 able to prevent PrP^C forming an intermolecular β-sheet? The average occurrence of protecting factors for edge strands in non-aggregating proteins is 2.5 [33], hence the β-bulge alone is unlikely to completely inhibit this kind of interaction. In addition, the shPrP X-ray structure [19] provides the experimental evidence that PrP^C can have edge-to-edge dimerization. In this structure, because of the crystal packing contacts, a PrP^C dimer with an intermolecular four stranded β-sheet is observed (Fig. 2A). However, this structure clarifies the βb1 role which is to limit the optimization of the intermolecular β-sheet; the sheet is indeed forced to adopt a marked twisting and only the two central intermolecular H-bonds are well optimized (O···H distance of 2.02 Å – black dot in Fig. 2A) whereas the two lateral H-bonds are distorted because of the bulge hindrance (O···H distance of 3.48 Å – red dot in Fig. 2A). Consistent with these unfavorable factors the β-sheet structure has very large atomic displacement parameters.

A different scenario is found when the dimer of the Q217R is modeled (Fig. 2B). In this case, the bulge is stretched and the β-sheet is elongated, allowing four intermolecular H-bonds to optimize their geometry (O···H distances within 1.8 Å and 2.2 Å). The bulge flattening not only supplies new H-bonds to the sheet, but also (Fig. 2B) seeds the extended conformations of the following residues which are prone to a further

Table 2
Main interactions in the W1 water binding site

	mPrP	chPrP	tlPrP	xlPrP
Water O	V161 Am	V168 Am	V161 Am	V161 Am
Water H	Q217 Sc	Q234 Sc	Q217 Sc	E221 Sc
Water H	S132 Carb	R139 Carb	S132 Carb	D132 Carb
βb1 Sc interactions[a]	S132 Sc-R220 Sc	R139 Sc-E237 Sc	S132 Sc-Q220 Sc	D132 Sc-R224 Sc
Gly Carb partner[b]	Q160 Sc-G131 Carb	R167 Sc-G138 Carb	Q160 Sc-G131 Carb	R160 Sc-G131 Carb

Abbreviations: amide "Am", SideChain "Sc", Carbonyl "Carb".
[a]Interaction that supports the bulge (see text).
[b]Interaction that prevents the β-sheet elongation (see text).

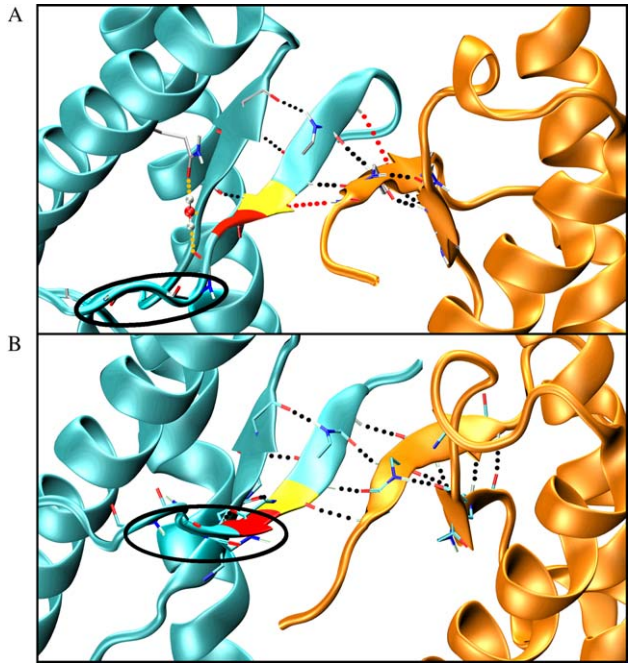

Fig. 2. Close up view of the intermolecular β-sheet in the crystal structure of shPrP (pdbcode: 1UW3) and its Q217R mutant (MD model [17]). (A) Ribbon representation of the shPrP(125–230) wild type dimer. Ribbon colour codes: cyan and orange for the two monomeric units, yellow for G131 and red for S132. The β-sheet presents the following H-bond network: 3 intramolecular H-bonds per each monomer (black dots), 2 optimized intermolecular H-bonds (black dots), and 2 distorted intermolecular H-bond (red dots). The W1 water is drawn for the cyan monomer (orange dots). The residues following the bulge are marked with a black ellipse. (B) Ribbon representation of the shPrP(125–230) Q217R dimer MD model [17]. Ribbon colour codes as in panel A. The dimer has been modelled from the monomeric Q217R MD model by using the crystal symmetries. Subsequently, an energy minimization procedure has been applied. β-sheet H-bonds network: 5 intramolecular H-bonds per each monomer (black dots) and 4 optimized intermolecular H-bonds (black dots). The residues following the stretched bulge are (black ellipse) prone to interact with the facing fragments and to produce an elongation of the sheet.

elongation of the sheet. Such regularity is evidently disrupted by the action of the bulge (Fig. 2A).

Finally we want to stress the role of the conserved hydration site in preserving βb1 structure. Consistent with the W1 stabilizing role, it turns out that the average value of the calculated free energy of binding is ~ -30 kJ mol^{-1} (calculated amongst the four PrP structure analyzed), rather high for a single water molecule. Moreover, shPrP simulations with the water removed have shown that the βb1 is destabilized, with fluctuations in the S132 position as large as 4 Å [17]. Overall, these data clearly show the link between local hydration and structural stability of βb1.

Since the dimerization has been repeatedly proposed to be the initial step in the PrP amyloidogenesis [36], it is important to focus on factors, like the βb1, that exert an influence on it. Our data show that this element is sensitive to the hydration state of the protein. It is likely that perturbations in the hydration of the environment may induce this conformational protection to fail, thus effectively increasing the PrP propensity to dimerization and aggregation.

3.3. Comparison of general hydration properties for mPrP and non-mPrP

The most intriguing aspect of the mPrPs hydration [17] is associated with protein surfaces (smooth spots) that are in contact with water in fast exchange with the bulk solution. These surfaces also show high entropy content for the solvent. These regions, which are the H1 and the C-terminal turns of the H2 and H3, in mPrPs may be potential *loci* for the protein interactions and aggregation (referred as L1, L2 and L3, respectively, Fig. 3B) owing to their lower desolvation energy.

Notably, for each identified *locus* a specific antibody interaction has been reported. The H2 C-term (L2) is the epitope of a sheep prion-monoclonal antibody as observed in the crystal structure [37], whereas another monoclonal antibody has shown to bind the C-terminal part of helix H3 (L3) of shPrP [38]. Consistent with the H1(L1) involvement in the PrP interactions, an antibody, which affects the prion propagation, is believed to target the β1-H1-β2 region [39].

When non-mPrPs are considered, it can be seen that the smooth spots L2 and L3 are not totally conserved (Fig. 3B). This is partially connected to the local differences in the sequence and structure. In particular the helix H2, that in huPrP and shPrP presents an unusual C-term tetra-threonine segment, is shorter in the chPrP and tPrP and it is kinked in xlPrP [18], whereas the H3 C-term segment is shorter in xlPrP and tPrP than the mPrPs. In addition, low sequence conservation is also found in the C-term turns of H2 and H3 compared to the higher conservation of the H1.

A direct comparison of the linearized protein hydration (LHF, Fig. 3B) identifies two PrP regions with a conserved hydration profile: a shallow valley, which is relative to the conserved smooth spots L1, and a huge peak corresponding to the W1. The residual part of the LHF plot does not show any common trends. Accordingly, H1 surface has conserved the hydration pattern resulting in the only smooth spot which is present in all the PrPs. This feature might have a functional

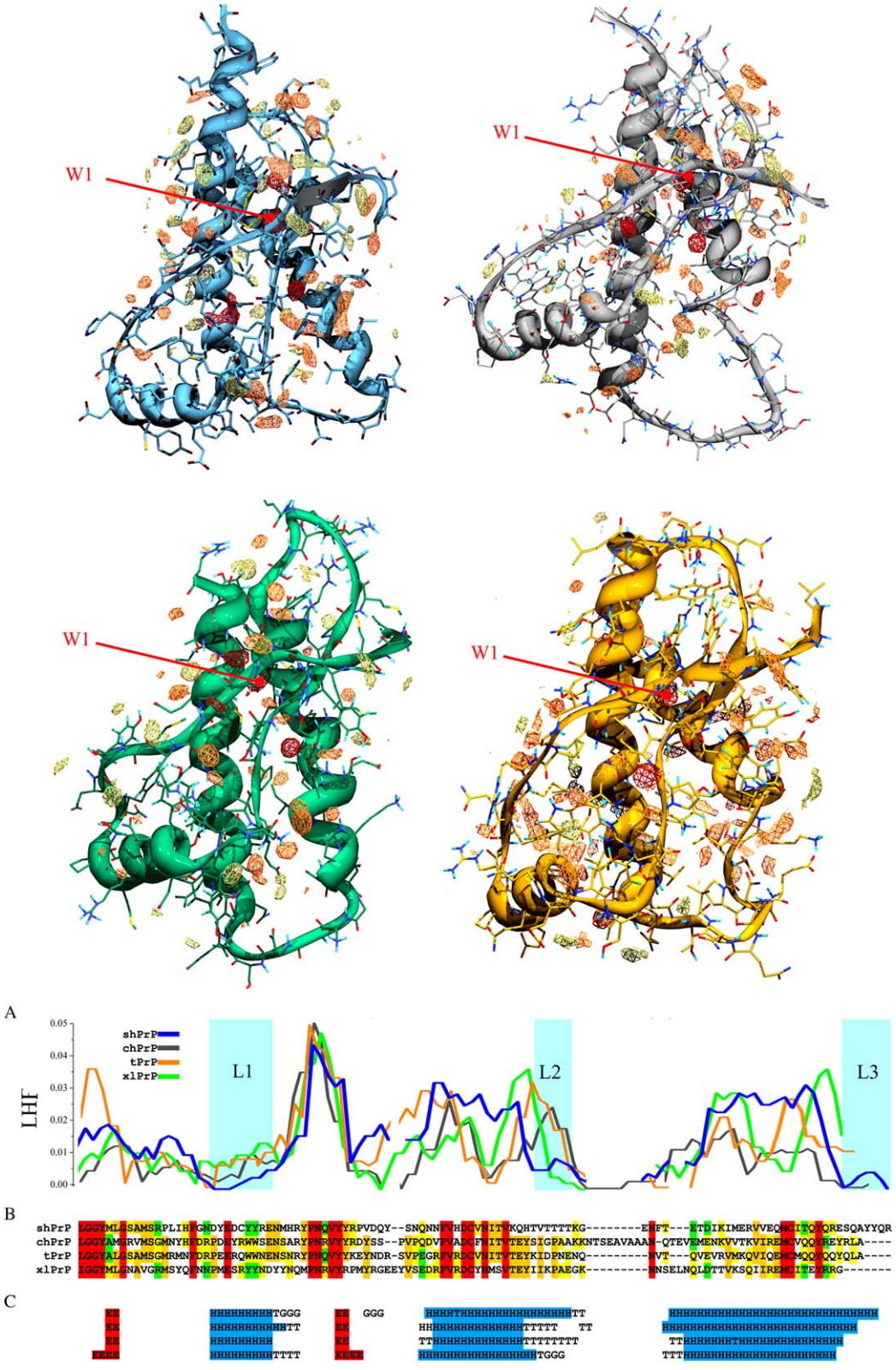

Fig. 3. PrPs hydration. (A) MDHS as water density maxima contoured at 2.5 times the bulk solvent density. Ribbon colour codes: shPrP cyan, chPrP silver, xlPrP green and tPrP orange. W1 water site is indicated in red. The shPrP presents wide spread MDHS except for the smooth spots (L1, L2 and L3). The chPrP hydration differs especially in the loop H2–H3, which appears poorly hydrated. This connecting loop, which is longer than in all other PrPs, is extremely mobile and would require a special treatment in the density map calculation. However we have no longer considered this loop in our analysis, since we want to focus on the hydration of regions with main chain H-bonds. (B) Linear hydration function (LHF). The location of smooth spots in mPrPs is evidenced by a cyan background and labelled. (C) Sequence alignment and secondary structure. The starting positions in the alignment are: 125-shPrP, 132-chPrP, 125-tPrP, 125-xlPrP. Colour codes: totally conserved residue: red, residues conserved among three structures: orange, residues conserved among two structures: yellow or green; secondary structure residues in α-helix: blue, residues in β-sheet: red.

relevance. In addition, the same region was previously noted for having a similar sequence pattern, conserved among PrPs, with the "EECYYDEN" fragment of human laminin α2 chain [18] (whose precursor receptor is a putative PrP^C partner [40–42]). Overall, these data support the idea of a possible involvement of the region in the PrP^C trafficking.

4. Summary

To our knowledge, this is the first MD analysis of PrPs sharing low sequence identity with the mPrPs. Our analyses focused on the hydration properties of the non-mPrPs and in particular on their influence on the folding stability and potential interaction *loci*. We studied a specific hydration site (W1) that brings together residues from three distant structural elements. Remarkably the site is conserved among the PrPs here analyzed, despite the sequence variability. We pointed out the structural role of the bound and buried water that appears to stabilize a conserved β-bulge; the latter is a conserved feature that might be "negatively designed" for preventing PrP^C aggregation. On the other hand, the comparison of the hydration maps of different PrPs demonstrates that the "smooth spot" at the H1 surface is a common characteristic of all PrP of known sequence and structure.

Acknowledgements: The authors thank Jens Kleinjung and Chandra Verma for critical reading of the manuscript. A.D.S. and A.Z. are grateful to Professor B. Salvato for having encouraged this work, to Professor L. De Arcangelis and Dr. A. De Candia for computational support, and acknowledge the M.I.U.R. COFIN03 (prot 2003 031424) and FIRB 2003.

Appendix A. Supplementary data

Supplementary data associated with this article can be found, in the online version, at doi:10.1016/j.febslet.2006.02.083.

References

[1] Martins, V.R., Linden, L., Prado, M.A., Walz, R., Sakamoto, A.C., Izquierdo, I. and Brentani, R.R. (2002) Cellular prion protein: on the road for functions. FEBS Lett. 512, 25–28.
[2] Prusiner, S.B. (1982) Novel proteinaceous infectious particles cause scrapie. Science 216, 136–144.
[3] Prusiner, S.B. (1998) Prions. Proc. Natl. Acad. Sci. USA 95, 13363–13383.
[4] Stahl, N., Baldwin, M.A., Teplow, D.B., Hood, L., Gibson, B.W., Burlingame, A.L. and Prusiner, S.B. (1993) Structural studies of the scrapie prion protein using mass spectrometry and amino acid sequencing. Biochemistry 32, 1991–2002.
[5] Govaerts, C., Wille, H., Prusiner, S.B. and Cohen, F.E. (2004) Evidence for assembly of prions with left-handed beta-helices into trimers. Proc. Natl. Acad. Sci. USA 101, 8342–8347.
[6] Nelson, R., Sawaya, M.R., Balbirnie, M., Madsen, A.O., Riekel, C., Grothe, R. and Eisenberg, D. (2005) Structure of the cross-beta spine of amyloid-like fibrils. Nature 435, 773–778.
[7] Sambashivan, S., Liu, Y., Sawaya, M.R., Gingery, M. and Eisenberg, D. (2005) Amyloid-like fibrils of ribonuclease A with three-dimensional domain-swapped and native-like structure. Nature 437, 266–269.
[8] Dobson, C.M. (2005) Structural biology: prying into prions. Nature 435, 747–749.
[9] Eghiaian, F. (2005) Structuring the puzzle of prion propagation. Curr. Opin. Struct. Biol. 15, 1–7.
[10] Dobson, C.M. (1999) Protein misfolding, evolution and disease. Trends Biochem. Sci. 24, 329–332.
[11] Fernandez, A. (2005) What factor drives the fibrillogenic association of beta-sheets? FEBS Lett. 579, 6635–6640.
[12] Fernandez, A. and Scheraga, H.A. (2003) Insufficiently dehydrated hydrogen bonds as determinants of protein interactions. Proc. Natl. Acad. Sci. USA 100, 113–118.
[13] Fernandez, A., Kardos, J., Scott, L.R., Goto, Y. and Berry, R.S. (2003) Structural defects and the diagnosis of amyloidogenic propensity. Proc. Natl. Acad. Sci. USA 100, 6446–6451.
[14] Fernandez, A. (2002) Insufficient hydrogen-bond desolvation and prion-related disease. Eur. J. Biochem. 269, 4165–4168.
[15] Cordeiro, Y., Kraineva, J., Ravindra, R., Lima, L.M., Gomes, M.P., Foguel, D., Winter, R. and Silva, J.L. (2004) Hydration and packing effects on prion folding and beta-sheet conversion. High pressure spectroscopy and pressure perturbation calorimetry studies. J. Biol. Chem. 279, 32354–32359.
[16] Grudzielanek, S., Jansen, R. and Winter, R. (2005) Solvational tuning of the unfolding, aggregation and amyloidogenesis of insulin. J. Mol. Biol. 351, 879–894.
[17] De Simone, A., Dodson, G.G., Verma, C.S., Zagari, A. and Fraternali, F. (2005) Prion and water: tight and dynamical hydration sites have a key role in structural stability. Proc. Natl. Acad. Sci. USA 102, 7535–7540.
[18] Calzolai, L., Lysek, D.A., Perez, D.R., Guntert, P. and Wuthrich, K. (2005) Prion protein NMR structures of chickens, turtles, and frogs. Proc. Natl. Acad. Sci. USA 102, 651–655.
[19] Haire, L.F., Whyte, S.M., Vasisht, N., Gill, A.C., Verma, C., Dodson, E.J., Dodson, G.G. and Bayley, P.M. (2004) The crystal structure of the globular domain of sheep prion protein. J. Mol. Biol. 336, 1175–1183.
[20] Berendsen, H.J.C., van der Spoel, D. and van Drunen, R. (1995) GROMACS: "A message-passing parallel molecular dynamics implementation". Comp. Phys. Commun. 91, 43–56.
[21] Van Gunsteren, W.F., Billeter, S., Eising, A., Hunenberger, P.H., Kruger, P., Mark, A.E., Scott, W.R.P. and Tironi, I.G. (1996) Biomolecular Simulations: The GROMOS96 Manual and User Guide. VdF: Hoshshulverlag AG an der ETH Zurich and BIOMOS b.v, Zurich, Gronigen.
[22] Berendsen, H.J.C., Postma, J.P.M., van Gunsteren, W.F. and Di Nola, A. (1984) Molecular dynamics with coupling to an external bath. J. Phys. Chem. 81, 3684–3690.
[23] Berendsen, H.J.C., Grigerra, J.R. and Straatsma, T.P. (1987) The missing term in effective pair potentials. J. Phys. Chem. 91, 6269–6271.
[24] Hess, B., Bekker, H., Berendsen, H.J.C. and Fraaije, J. (1997) LINCS: A linear constraint solver for molecular simulations. J. Comput. Chem. 18, 1463–1472.
[25] Darden, T., Perera, L., Li, L. and Pedersen, L. (1999) New tricks for modelers from the crystallography toolkit: the particle mesh Ewald algorithm and its use in nucleic acid simulations. Struct. Fold Des. 7, R55–R60.
[26] Lounnas, V. and Pettitt, B.M. (1994) Distribution function implied dynamics versus residence times and correlations: solvation shells of myoglobin. Proteins 18, 148–160.
[27] Lounnas, V., Pettitt, B.M. and Phillips Jr., G.N. (1994) A global model of the protein–solvent interface. Biophys. J. 66, 601–614.
[28] Hamelberg, D. and McCammon, J.A. (2004) Standard free energy of releasing a localized water molecule from the binding pockets of proteins: double-decoupling method. J. Am. Chem. Soc. 126, 7683–7689.
[29] Fraternali, F. and Cavallo, L. (2002) Parameter optimized surfaces (POPS): analysis of key interactions and conformational changes in the ribosome. Nucleic Acids Res. 30, 2950–2960.
[30] Liemann, S. and Glockshuber, R. (1999) Influence of amino acid substitutions related to inherited human prion diseases on the thermodynamic stability of the cellular prion protein. Biochemistry 38, 3258–3267.
[31] Panegyres, P.K., Toufexis, K., Kakulas, B.A., Cernevakova, L., Brown, P., Ghetti, B., Piccardo, P. and Dlouhy, S.R. (2001) A

new PRNP mutation (G131V) associated with Gerstmann–Straussler–Scheinker disease. Arch. Neurol. 58, 1899–1902.
[32] Fernandez-Escamilla, A.M., Rousseau, F., Schymkowitz, J. and Serrano, L. (2004) Prediction of sequence-dependent and mutational effects on the aggregation of peptides and proteins. Nat. Biotechnol. 22, 1302–1306.
[33] Richardson, J.S. and Richardson, D.C. (2002) Natural beta-sheet proteins use negative design to avoid edge-to-edge aggregation. Proc. Natl. Acad. Sci. USA 99, 2754–2759.
[34] Santini, S., Claude, J.B., Audic, S. and Derreumaux, P. (2003) Impact of the tail and mutations G131V and M129V on prion protein flexibility. Proteins 51, 258–265.
[35] Jin, T., Gu, Y., Zanusso, G., Sy, M., Kumar, A., Cohen, M., Gambetti, P. and Singh, N. (2000) The chaperone protein BiP binds to a mutant prion protein and mediates its degradation by the proteasome. J. Biol. Chem. 275, 38699–38704.
[36] Kaneko, K., Zulianello, L., Scott, M., Cooper, C.M., Wallace, A.C., James, T.L., Cohen, F.E. and Prusiner, S.B. (1997) Evidence for protein X binding to a discontinuous epitope on the cellular prion protein during scrapie prion propagation. Proc. Natl. Acad. Sci. USA 94, 10069–10074.
[37] Eghiaian, F., Grosclaude, J., Lesceu, S., Debey, P., Doublet, B., Treguer, E., Rezaei, H. and Knossow, M. (2004) Insight into the $PrP^{C} \rightarrow PrP^{Sc}$ conversion from the structures of antibody-bound ovine prion scrapie-susceptibility variants. Proc. Natl. Acad. Sci. USA 101, 10254–10259.
[38] Peretz, R. et al. (1997) A conformational transition at the N terminus of the prion protein features in formation of the scrapie isoform. J. Mol. Biol. 273, 614–622.
[39] Heppner, F.L. et al. (2001) Prevention of scrapie pathogenesis by transgenic expression of anti-prion protein antibodies. Science 294, 178–182.
[40] Graner, E. et al. (2000) Cellular prion protein binds laminin and mediates neuritogenesis. Brain Res. Mol. Brain Res. 76, 85–92.
[41] Gauczynski, S. et al. (2001) The 37-kDa/67-kDa laminin receptor acts as the cell-surface receptor for the cellular prion protein. EMBO J. 20, 5863–5875.
[42] Rieger, R., Edenhofer, F., Lasmezas, C.I. and Weiss, S. (1997) The human 37-kDa laminin receptor precursor interacts with the prion protein in eukaryotic cells. Nat. Med. 3, 1383–1388.